

# PSO-BASED TMD & ATMD CONTROL FOR HIGH-RISE STRUCTURE EXCITED BY SIMULATED FLUCTUATING WIND FIELD

W. Huang<sup>1,3</sup> – D. Y. Zhu<sup>1,3\*</sup> – J. Xu<sup>2</sup> – X. J. Wang<sup>1,3</sup> – J. W. Lu<sup>4</sup> – K. L. Lu<sup>1,3</sup>

<sup>1</sup> School of Civil and Hydraulic Engineering, Hefei university of technology, Hefei, China

<sup>2</sup> China National Machinery Industry Corporation, Beijing, China

<sup>3</sup> Anhui Provincial Laboratory of Civil Engineering and Materials, Hefei, China

<sup>4</sup> School of Mechanical and Automotive Engineering, Hefei university of technology, Hefei, China

## ARTICLE INFO

### Article history:

Received: 19.05.2014.

Received in revised form: 13.08.2014.

Accepted: 27.08.2014.

### Keywords:

Decimation-in-time

Fast Fourier transform

Waves with weighted amplitude

Wind speed spectrum

Benchmark structure

Tuned mass damper

Active tuned mass damper

Linear quadratic Gaussian algorithm

Integral of the absolute value of the error

Particle swarm optimization algorithm

## Abstract:

*This paper reports a novel control strategy combined with artificial intelligence for wind-induced vibration control of a high-rise structure and also provides a broader idea for traditional structural vibration control. The fast Fourier transform based on decimation-in-time was used to optimize the waves with a weighted amplitude method, and the wind speed field was numerically generated according to a Davenport - type fluctuating wind speed spectrum. A second-generation benchmark structure was selected as the high-rise building model. Tuned mass damper (TMD) and active tuned mass damper (ATMD) served as the controller, and the linear-quadratic-Gaussian algorithm served as the active control algorithm for ATMD. Simultaneously, the particle swarm optimization algorithm was introduced, and the integral of the absolute value of the error based on the relative displacement of floors with regard to the ground level was defined as a performance index for optimizing. The numerical results reveal that both of the two proposed controllers have excellent capability in reducing wind-induced vibrations in high-rise buildings; moreover, the PSO-based ATMD performed better than PSO-based TMD.*

## 1 Introduction

With the rapid development of high-rise buildings, more and more attention has been paid to wind-induced vibrations so that effective control strategies have been developed for comfort and safety. In general, they are classified as active,

semi-active, passive, and hybrid control methods. Tuned mass damper (TMD) is one of the oldest passive control devices, first reported by Framh [1]. Rana and Soong [2] performed a parametric study for enhancing the understanding of some important characteristics of TMD. A standard SDOF (single

\* Corresponding author. Tel.: +86 551 6291 9186  
E-mail address: zhudymeng@163.com

degree of freedom) system has been used to develop two different optimization criteria for TMD [3]. Bekdaş and Nigdeli [4] used a Harmony Search (HS), i.e. a meta-heuristic optimization method, to determine the optimal parameters of TMD.

Concomitantly, active tuned mass dampers (ATMDs) have emerged due to the various restrictions of TMD such as a not ideal control effect. Abdel [5] reported a process for designing optimal ATMD. An adopted control scheme consisted of an ATMD where the control action was achieved by a fuzzy logic controller (FLC); its ability to handle any nonlinear behavior was also studied [6].

In general, the simulation strategies of a random fluctuating wind can be divided into two types: (i) linear regression filtering techniques such as the auto regressive (AR) method [7] and autoregressive moving average (ARMA) method [8–10] and (ii) the harmonic synthesis method based on trigonometric series superposition. The former has a small amount of computation but poor accuracy; in contrast, the latter has a higher precision with unconditional stability. Shinozuka and Jan [11] simulated a random wind field by waves with weighted amplitude (WAWS), and then the structural responses were computed. Recently, several studies on further improving WAWS have been conducted to improve efficiency. YANG [12] applied fast Fourier transform (FFT) to WAWS for the first time, thus significantly improving the efficiency of harmonic terms superposition. For further improving the efficiency of FFT, SUN [13] used a decimation-in-time (DIT) strategy (a signal processing technique) to accelerate the superposition.

In general, a traditional gradient-based optimization method requires computations of sensitivity factors and eigenvectors in its iterative process. This causes heavy computational burden and slow convergence. Moreover, there is no local criterion to distinguish whether a local solution is also the global solution. Thus, conventional optimization methods using derivatives and gradients are generally not able to locate or identify the global optimum with certainty; however, for real-world applications, one is often content with a good solution even if it is not the best solution. Consequently, heuristic methods are widely used for the global optimization problem. Particle swarm optimization (PSO) algorithm was first proposed by Eberhart and Kennedy [14], and it

is novel population-based metaheuristic utilizing the swarm intelligence generated by the cooperation and competition between the particles in a swarm, which has emerged as a useful tool for engineering optimization.

## 2 Fluctuating wind speed field simulation using DIT-FFT-WAWS method

### 2.1 Brief introduction to WAWS

A  $M$ -dimensional, zero mean, stationary, and random process is expressed as follows:

$$v(t) = \{v_1(t), v_2(t), \dots, v_M(t)\}^T. \quad (1)$$

Further, the cross-spectral density function matrix is expressed as follows:

$$S(f) = \begin{bmatrix} s_{11}(f) & s_{12}(f) & \dots & s_{1M}(f) \\ s_{21}(f) & s_{22}(f) & \dots & s_{2M}(f) \\ \dots & \dots & \dots & \dots \\ s_{M1}(f) & s_{M2}(f) & \dots & s_{MM}(f) \end{bmatrix}, \quad (2)$$

where,  $S_{ii}(f)$  and  $S_{ij}(f)$  are the self-spectral density function matrix and cross-spectral density function matrix, respectively,  $i, j = 1, 2, \dots, M$ ; the Cholesky decomposition of Eq. (2) can be performed as follows:

$$S(f) = H(f)H^*(f)^T, \quad (3)$$

$$H(f) = \begin{bmatrix} H_{11}(f) & 0 & \dots & 0 \\ H_{21}(f) & H_{22}(f) & \dots & 0 \\ \dots & \dots & \dots & \dots \\ H_{M1}(f) & H_{M2}(f) & \dots & H_{MM}(f) \end{bmatrix}, \quad (4)$$

where,  $H(f)$  and  $H^*(f)$  are conjugate transpose matrices, and their elements have the following properties:

$$H_{jj}(f) = H_{jj}(-f), \quad j = 1, 2, \dots, M \quad (5)$$

$$H_{ij}(f) = |H_{ij}^*(f)| e^{i\theta_{ij}(f)}, \quad (6)$$

$$\theta_{ij}(f) = \tan^{-1} \left( \frac{\text{Im}(H_{ij}(f))}{\text{Re}(H_{ij}(f))} \right), \quad (7)$$

$$i = 1, 2, \dots, M \quad ; \quad j = 1, 2, \dots, i-1 \quad ; \quad i > j.$$

Stochastic process vector  $v(t)$  can be defined as follows:

$$v_i(t) = \sum_{j=1}^i \sum_{l=1}^N |H_{ij}(f_{jl})| \cdot \sqrt{2\Delta\omega} \cos[2\pi f_{jl}t + \theta_{ij}(f_{jl}) + \Phi_{jl}], \quad (8)$$

$i = 1, 2, \dots, M.$

In Eq. (8),  $f_{jl} = \frac{\omega_{jl}}{2\pi} = \frac{(l-1/2)\Delta\omega}{2\pi}$ , the frequency increment is  $\Delta\omega = \omega_{up}/N$ , and  $N$  is a positive and large integer.  $\omega_{up}$  is the cutoff frequency, and it should be selected according to the actual frequency characteristics of the target structure.  $\Phi_{jl}$  is a random number between 0 and  $2\pi$ . Moreover, the time step  $\Delta t$  should satisfy Eq. (9) in order to prevent aliasing between mutually adjacent frequencies when the wind speed data are generated by Eq. (8).

$$\Delta t \leq \pi / \omega_{up}. \quad (9)$$

Eq. (3) shows a very large amount of computation, because the Cholesky decomposition must be performed for each frequency  $f$ .

## 2.2 DIT-FFT-WAWS method

Dividing the  $N = 2^\beta$  sequences  $x(i)$  ( $i = 0, 1, 2, \dots, N-1$ ) into two parts:

$$\begin{cases} x(2j) = x_1(j) \\ x(2j+1) = x_2(j) \end{cases} \quad (j = 0, 1, 2, \dots, \frac{N}{2} - 1). \quad (10)$$

The discrete Fourier transform (DFT) of the front and rear halves of the shown sequences can be achieved as follows:

$$X(k) = X_1(k) + W^k X_2(k) \quad (k = 0, 1, 2, \dots, \frac{N}{2} - 1), \quad (11)$$

$$X(k + \frac{N}{2}) = X_1(k) - W^k X_2(k) \quad (k = 0, 1, 2, \dots, \frac{N}{2} - 1), \quad (12)$$

where,  $W = \exp(-j4\pi/N)$ ,  $j$  is the imaginary unit. By repeating the above process, the FFT form of  $x(i)$  can be obtained.

The analysis shows that the computation amount is proportional to  $N^2$  when the direct operation is

performed; however, it is proportional to  $N \log_2 N$  if DIT-FFT is used.

For introducing DIT-FFT, Eq. (8) can be rewritten as follows:

$$y_i(p\Delta t) = \sqrt{2\Delta\omega} \sum_{i=1}^j M_{ij}(p\Delta t) \exp\left[i\left(\frac{j\Delta\omega}{2} p\Delta t\right)\right], \quad (13)$$

$$\text{where } M_{xy}(p\Delta t) = \sum_{l=1}^{2N-1} B_{xy}(l\Delta\omega) \exp\left[i\left(\frac{2\pi pl}{2N}\right)\right], \quad (14)$$

$$B_{ij}(l\Delta\omega) = \begin{cases} H_{ij}(l\Delta\omega + \frac{1}{2}\Delta\omega) \exp(i\Phi_{ij}), & 0 \leq l \leq N \\ 0, & N \leq l \leq 2N \end{cases}. \quad (15)$$

Then, Eq. (14) is accelerated using the DIT-FFT-WAWS technique:

$$M_{ij}(p\Delta t) = \text{DIT-FFT}[B_{ij}(l\Delta\omega)]. \quad (16)$$

In Eq. (16), **DIT-FFT**[ $\cdot$ ] denotes the FFT based on DIT technique.

## 3 TMD and ATMD control for 76-story benchmark structure

### 3.1 76-Story benchmark structure

The tall building considered was a 76-story 306.1 m office tower proposed for the city of Melbourne, Australia, and the schematic diagram is shown in Fig. 1 [15]. The total mass of the building, including heavy machinery in the plant rooms, is 153,000 t. The total volume of the building is 510,000 m<sup>3</sup>, resulting in a mass density of 300 kg/m<sup>3</sup>, which is typical of concrete structures. The building is slender with a height-to-width ratio of 7.3; therefore, it is wind sensitive. Moreover,  $\bar{v}_{10} = 15$  m/s, the ground roughness coefficient  $\alpha = 0.03$ , atmospheric density = 1.25 kg/m<sup>3</sup>, and the geomorphologic factor = 0.4. The shape coefficients can be obtained from "Load code for the design of building structures", [16] as shown in Fig. 2.

An order reduction operation should be performed for the original model so as to avoid an overly complex analysis. Moreover, the condensation model also preserved the dynamic characteristics of the original structure well. Besides, sensors were

installed at the floors of 1, 30, 50, 55, 60, 65, 70, 75, and 76.

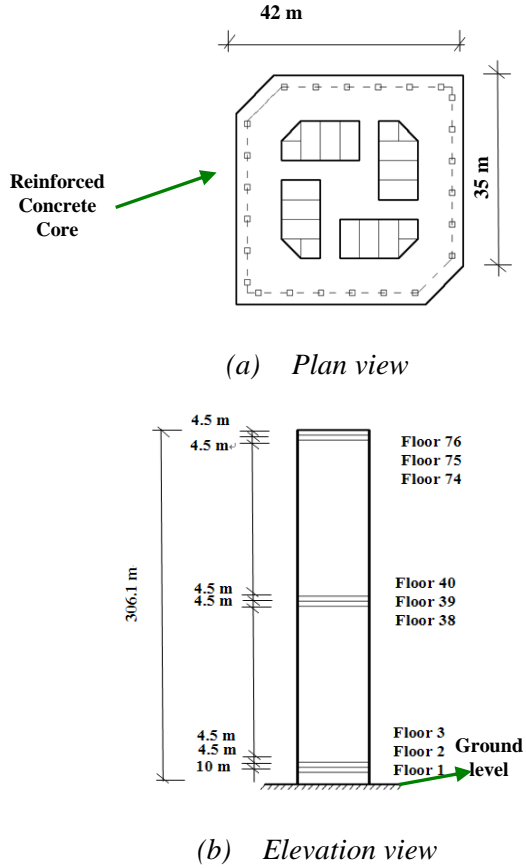


Figure 1. Schematic diagram of the benchmark structure.

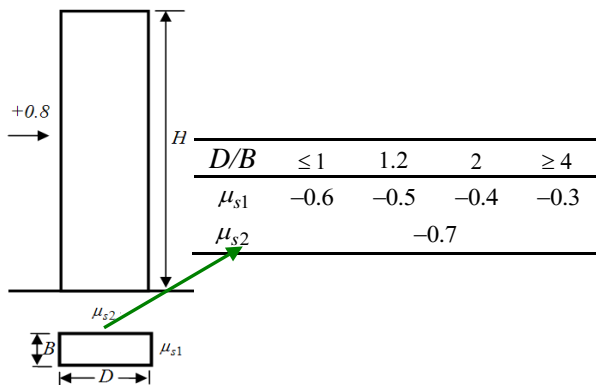


Figure 2. Diagrammatic sketch of shape coefficients.

### 3.2 Numerical simulation of fluctuating wind speed field

In this study, Davenport fluctuating wind speed field [17] was simulated, and the self-spectral density function can be denoted as follows:

$$S_{ii}(f) = 4\alpha \bar{v}_{10}^{-2} \frac{x^2}{f(1+x^2)^{4/3}}, \quad (17)$$

where,  $x = \frac{1200f}{\bar{v}_{10}}$  is the turbulence integral scale factor,  $f$  is the frequency of the fluctuating wind,  $\alpha$  is the ground roughness coefficient, and  $\bar{v}_{10}$  is the average wind speed at 10 m height.

The cross-spectral density function of the two random floors  $\langle m, n \rangle$  of the benchmark structure can be expressed as follows:

$$S_{mn}(f) = \sqrt{S_{mm}(f)S_{nn}(f)} \cdot ch(f) \cdot e^{i\Psi(f)}, \quad (18)$$

where,  $ch(f)$  is the coherence function, and only the downwind planes are considered in this study; thus,  $ch(f)$  can be expressed as follows:

$$ch(f) = \exp \left[ \frac{-2f \cdot \sqrt{c_x^2(x_i - x_j)^2 + c_z^2(z_i - z_j)^2}}{\bar{v}(z_i) + \bar{v}(z_j)} \right], \quad (19)$$

$(x_i, z_i), (x_j, z_j)$  are the coordinates of the considered planes,  $c_x, c_z$  are the attenuation coefficients, and  $c_x = 6, c_z = 10$ .

Finally, the phase angle  $\Psi(f)$  can be determined as follows:

$$\Psi(f) = \begin{cases} \frac{\pi f \Delta z}{4V(z)} & \frac{f \Delta z}{V(z)} \leq 0.1 \\ 1.25 - \frac{10\pi \Delta z}{V(z)} & 0.1 < \frac{f \Delta z}{V(z)} \leq 0.125 \\ rand & \frac{f \Delta z}{V(z)} > 0.125 \end{cases} \quad (20)$$

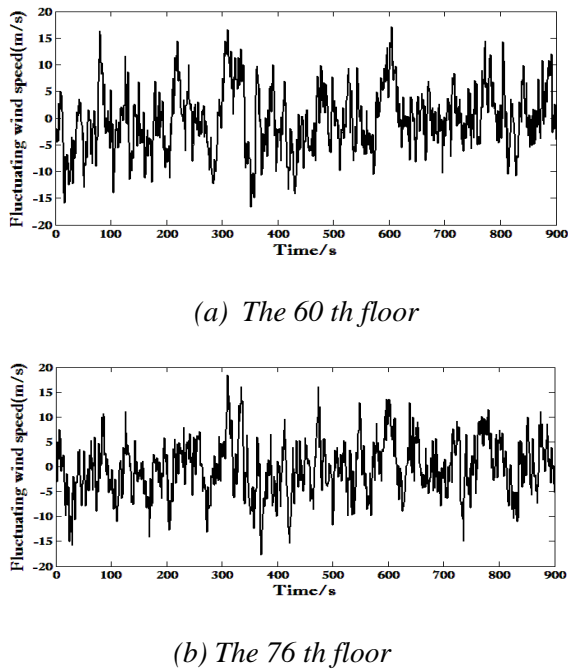


Figure 3. Wind speed field.

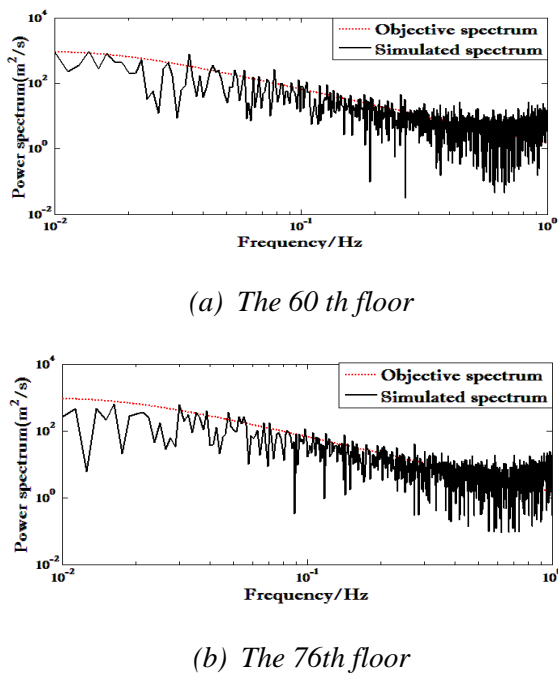


Figure 4. Spectral density function curves.

Figs. 3 and 4 show the speed process and spectral density function curves of the 60 th and 76 th floor of the benchmark structure. Clearly, compared to the Davenport-like objective spectrum, the simulated spectrum is almost the same as the trend and peak value. Therefore, it is feasible to simulate the fluctuating wind for the benchmark structure

using DIT-FFT-WAWS. The fluctuating wind load processes are shown in Fig. 5.

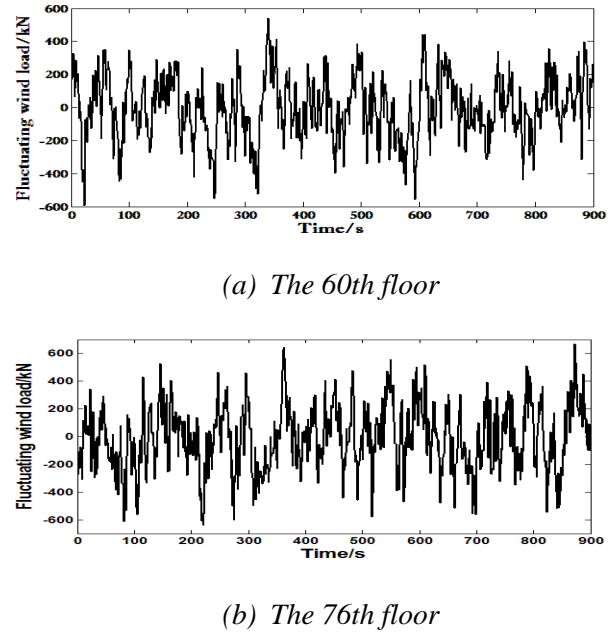


Figure 5. Fluctuating wind load.

### 3.3 TMD and ATMD control

#### 3.3.1 TMD control

A high-rise building with  $n$  stories is considered here, and TMD is applied on the  $k$  th floor. The motion equations are formulated as follows:

$$\begin{cases} M \ddot{X} + C \dot{X} + KX = F_{TMD} + F_{wind} \\ m_d \ddot{x}_d + c_d (\dot{x}_d - \dot{x}_k) + k_d (x_d - x_k) = 0 \end{cases}, \quad (21)$$

where,  $M, C$ , and  $K$  are the mass, damping, and stiffness matrix of the tall building, respectively;  $X, \dot{X}, \ddot{X}$  are the structure displacement, velocity, and acceleration matrix, respectively;  $m_d, k_d$ , and  $c_d$  are the mass, damping, and stiffness of the TMD;  $x_d$  is the displacement of the TMD; and  $x_k$  is the displacement of the  $k$  th floor. The control force generated by the TMD can be denoted as follows:

$$F_{TMD} = \left[ 0, \dots, 0, k_d(x_d - x_k) + c_d(\dot{x}_d - \dot{x}_k), 0, \dots, 0 \right]^T \quad (22)$$

#### 3.3.2 ATMD control with LQG algorithm

Similar dynamic equations can be derived as follows:

$$\begin{cases} M \ddot{X} + C \dot{X} + KX = F_{wind} + EU \\ m_d \ddot{x}_d + c_d (\dot{x}_d - \dot{x}_k) + k_d (x_d - x_k) = F_{actuator} \end{cases}, \quad (23)$$

where,  $F_{wind}$  is the wind load vector,  $U$  is the control force vector,  $E$  is the location matrix of the control force,  $F_{actuator}$  is the control force exerted on the structure and the ATMD system.

Eq. (23) can be expressed as the state space form:

$$\begin{cases} \dot{Z} = AZ + BU + DF_{wind}(t) + \varepsilon_1(t), Z(0) = 0 \\ Y = C_0AZ + C_0BU + \varepsilon_2(t) \end{cases}, \quad (24)$$

where,  $\varepsilon_1(t), \varepsilon_2(t)$  are the input noise and measurement noise, respectively, and both of them are zero-mean Gaussian white-noise process.

First, the control force  $U(t)$  can be designed by the LQR (linear quadratic Gaussian) algorithm, namely,

$$U(t) = -GZ(t), \quad (25)$$

where,  $G$  is the gain matrix of the continuous state space equations.

Then, the full state of the structure was estimated according to the observed output and the Kalman filter, and the objective function can be selected as follows:

$$J_e = E \left[ \{Z(t) - \hat{Z}(t)\}^T \{Z(t) - \hat{Z}(t)\} \right], \quad (26)$$

where,  $\hat{Z}(t)$  is the estimation of the  $Z(t)$ ; Kalman filter and filter gain  $K_e$  can be constructed by minimizing the objective function as follows:

$$\begin{cases} \dot{\hat{Z}} = A\hat{Z} + BU + K_e(Y - \hat{Y}) \\ \hat{Z}(t_0) = \hat{Z}_0, \hat{Y} = C_0\hat{Z} \end{cases}, \quad (27)$$

with the obtained feedback gain  $G$  and the Kalman filter gain  $K_e$ , the following state equations can be derived as follows:

$$\begin{cases} \dot{\hat{Z}} = (A - BG - K_e C_0 A + K_e C_0 B G) \hat{Z} + K_e Y + DF_{wind} \\ Y = C_0(\hat{Z} - DF), Z(0) = 0 \end{cases}. \quad (28)$$

## 4 PSO-based TMD and ATMD control

### 4.1 PSO algorithm

The updated equations of the particle velocities and positions are the core parts in the PSO algorithm and can be denoted as follows:

$$v_{ij} = \omega v_{ij}(t) + c_1 r_1 (pbest_{ij}(t) - x_{ij}(t)) + c_2 r_2 (gbest_{ij}(t) - x_{ij}(t)), \quad (29)$$

$$x_{ij}(t+1) = x_{ij}(t) + v_{ij}(t+1), \quad (30)$$

where,  $i$  represents the  $i$ th particle;  $j$  represents the  $j$ th dimension of each particle;  $v_{ij}(t)$  represents the flight velocity component of the  $j$ th dimension in the evolution of  $t$ th generation;  $x_{ij}(t)$  represents the flight displacement component of the  $j$ th dimension in the evolution of  $t$ th generation;  $pbest_{ij}(t)$  represents the optimal location component of the  $j$ th dimension in the evolution of the  $t$ th generation of particle  $i$ ;  $gbest_j(t)$  represents the  $j$ th dimension of the optimal position of the entire particle swarm in the evolution of the  $t$ th generation;  $c_1, c_2$  are acceleration factors or learning factors; and  $r_1, r_2$  are random numbers between (0,1).  $\omega$  is the inertia weight factor and plays a key role in the PSO for global optimum, and a linear changing strategy is often used as reported by Shi and Eberhart [18]. However, a simple and effective form of  $\omega$  is introduced here, namely,  $\omega = 0.99^t$  [19].

### 4.2 Performance index

During the TMD or ATMD control, the entire time  $T_f$  can be discrete with an equal step  $\Delta t$ , and the performance index, namely, the integral of absolute value of error (IAE) can be defined as follows:

$$IAE_i = \sum_{t=1\Delta t}^{T_f} |x_i(t)|, \quad (31)$$

where  $t = k\Delta t$  is an arbitrary discrete time;  $x_i$  is the displacement of the  $i$ th floor w.r.t. ground level and also the error in the proposed control;  $T_f = 900s$ ,  $\Delta t = 0.1s$ . Finally, the fitness function is defined as follows:

$$J = \sum_{i=1}^{76} IAE_i \quad (32)$$

By performing this index, the overall displacement of the tall building (summation of every floor displacement) in the entire time process can be reduced, consistent with the final purpose of the wind-induced control of a high-rise structure.

The procedure of the PSO-based TMD and ATMD control strategy is shown in Fig. 6, and the design variables, constraints, and PSO settings of the entire optimization are shown in Section 5 for the case studies.

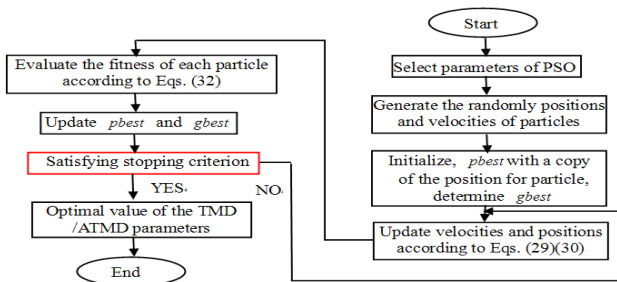


Figure 6. Flowchart of PSO-based TMD/ATMD control

### 5 Case studies

To investigate the performance of the proposed control strategy, the PSO-based TMD/ATMD strategy was applied to the benchmark structure, and the main idea is mentioned above.

The frequency ratio of TMD (ATMD) to the first-order frequency of the main structure is denoted as  $\beta_{ratio}$ , the mass ratio to the total mass of the building is denoted as  $m_{ratio}$ , and the damping ratio is denoted as  $\zeta_{ratio}$ .

For the PSO-based TMD,  $m_{ratio}$ ,  $\beta_{ratio}$ , and  $\zeta_{ratio}$  were optimized by evaluating the cost function as shown in Eq. (33). Further, the number of particles, particle size, number of iteration, and  $c_1, c_2$  were selected as 100, 3, 50, 2.0, and 2.0.

$$Particle = [\underline{\dim(1), \dim(2), \dim(3)}] \\ m_{ratio}, \beta_{ratio}, \zeta_{ratio}$$

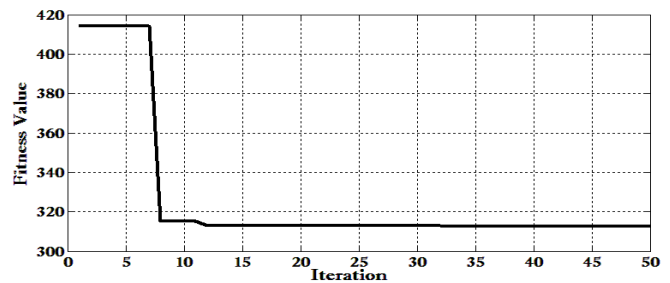
$$Constraints: \begin{cases} 0.001 \leq m_{ratio} \leq 0.009 \\ 0.001 \leq \zeta_{ratio} \leq 0.900 \\ 0.100 \leq \beta_{ratio} \leq 10.000 \end{cases} \quad (33)$$

For the PSO-based ATMD,  $m_{ratio}$ ,  $\beta_{ratio}$ ,  $\zeta_{ratio}$ , and weight matrix  $Q, R$  were optimized by evaluating the cost function as shown in Eq. (34), and the number of particles, particle size, number of iteration, and  $c_1, c_2$  were similarly set as 100, 34, 50, 2.0, and 2.0.

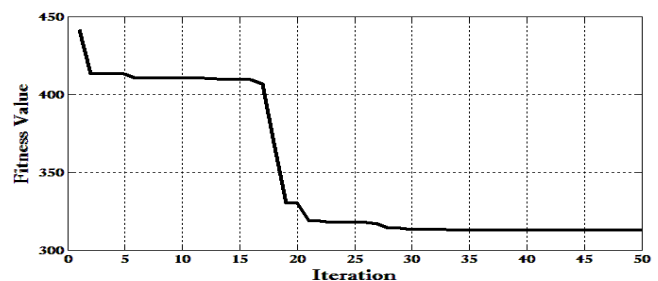
$$Particle = [\underline{\dim(1), \dim(2), \dim(3), \dim(4), \dots, \dim(33), \dim(34)}] \\ m_{ratio}, \beta_{ratio}, \zeta_{ratio} \quad q \quad R$$

$$q = [\dim(4), \dots, \dim(33)], Q = \text{diag}(q).$$

$$Constraints: \begin{cases} 0.001 \leq m_{ratio} \leq 0.009 \\ 0.001 \leq \zeta_{ratio} \leq 0.900 \\ 0.100 \leq \beta_{ratio} \leq 10.000 \\ 1 \leq q_i \leq 1 \times 10^5, (i = 1 \sim 30) \\ 0.01 \leq R \leq 1 \end{cases} \quad (34)$$



(a) PSO-based TMD

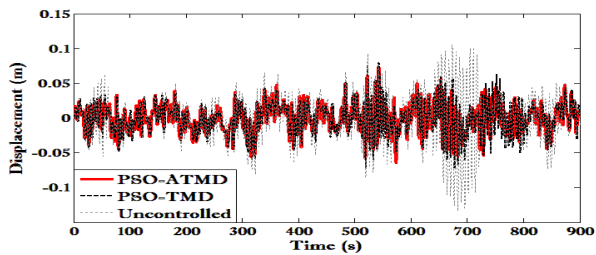


(b) PSO-based ATMD

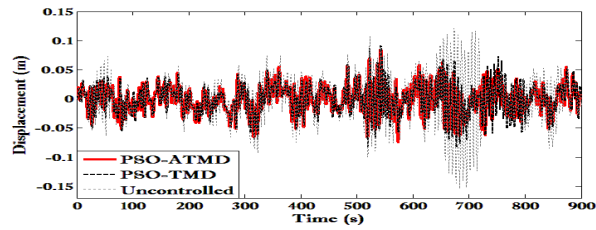
Figure 7. Fitness convergence.

Table 1. Optimal parameters

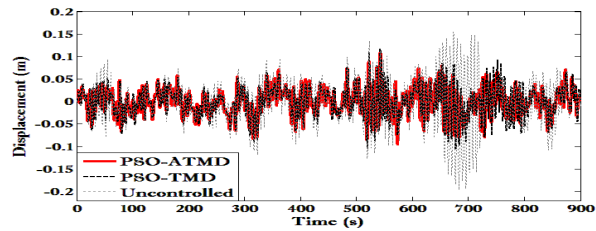
PSO-based TMD
$m_{ratio} = 0.009; \zeta_{ratio} = 0.0941; \beta_{ratio} = 1.022 .$
PSO-based ATMD
$m_{ratio} = 0.009; \zeta_{ratio} = 0.0946; \beta_{ratio} = 1.031 ;$ $Q = \text{diag}[0.907, 0.0001, 0.939, 0.344, 0.963, 0.0555, 1.000,$ $0.00001, 1.000, 0.0354, 0.951, 1.000, 0.0292, 0.0325, 0.929,$ $0.427, 0.376, 0.954, 0.922, 0.0171, 0.0736, 1.000, 0.197, 0.511,$ $0.00001, 0.465, 0.248, 0.850, 0.856, 0.0292] \times 10^5$ $R = 0.901 .$



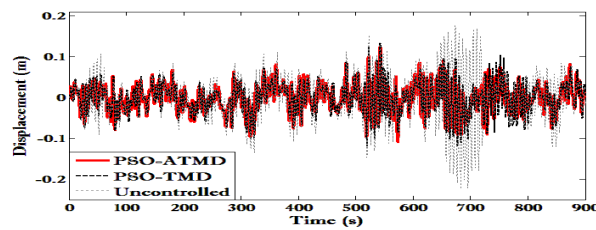
(a) The 55th floor



(b) The 60th floor

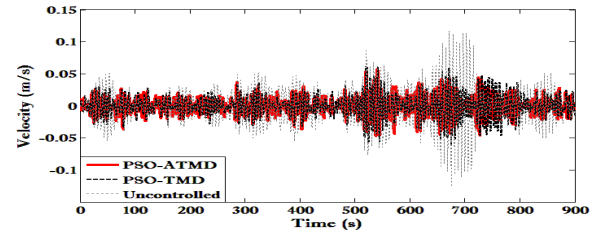


(c) The 70th floor

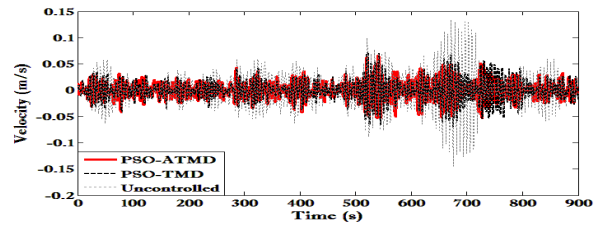


(d) The 76th floor

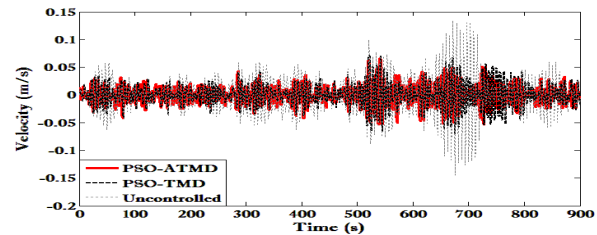
Figure 8. Structure displacement for comparison.



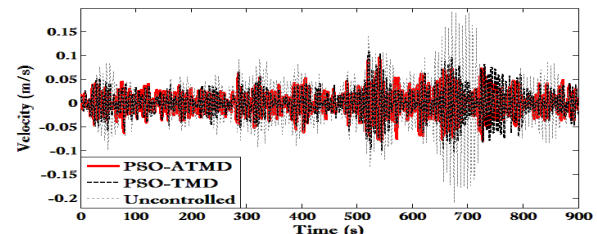
(a) The 55th floor



(b) The 60th floor



(c) The 70th floor



(d) The 76th floor

Figure 9. Structure velocity for comparison.

As shown in Table 1,  $m_{ratio}, \beta_{ratio}, \zeta_{ratio}$  are almost the same for two different strategies, indicating that the optimal parameters of the mass damper system is consistent with each other. Thus, the active algorithm may play a decisive role as shown in Figs. 8 and 9.

When comparing with the original study of the benchmark structure, the parameters were set as the same with the reference to [15], namely, TMD mass =  $500\alpha$ , the natural frequency =  $0.16\text{Hz}$ , and the damping ratio =  $0.2$ , the weighting matrix

$Q = \text{diag}[1,1,1, 1,1,1,1,1, 1,0,1,1,1,1,1,10^5,10^5,10^5,10^5,0,1,1,1,1, 10^5,10^5,10^5,10^5,0], R = 15 \times 10^{-2}$ , and the peak

responses under different working conditions are listed in Table 2.

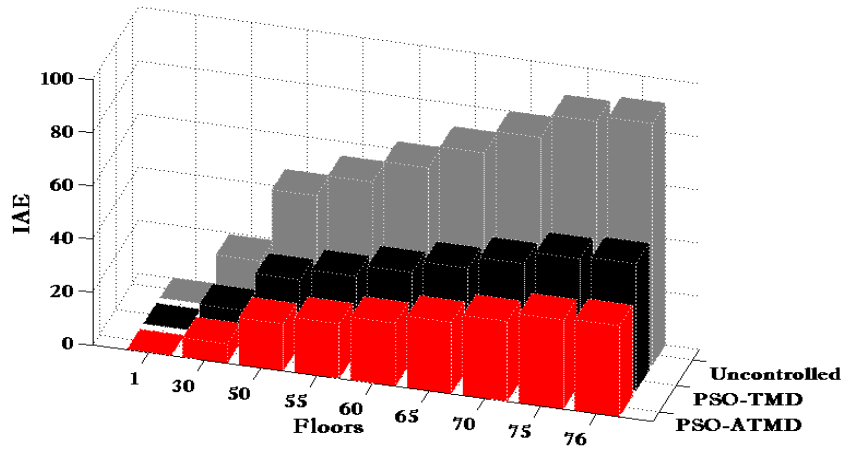


Figure 10. IAE index for comparison.

Table 2. Peak values (a-c)

(a) Peak displacement (cm)

Building floor	Uncontrolled	TMD	PSO-TMD	Reduction (%)	ATMD	PSO-ATMD	Reduction (%)
55	13.349	8.916	7.930	40.595	7.718	7.336	45.045
60	15.395	10.257	9.141	40.624	8.905	8.467	45.002
70	19.662	13.039	11.669	40.652	11.390	10.838	44.878
76	22.396	14.817	13.290	40.659	12.987	12.363	44.798

(b) Peak velocity (cm/s)

Building floor	Uncontrolled	TMD	PSO-TMD	Reduction (%)	ATMD	PSO-ATMD	Reduction (%)
55	12.582	8.215	6.127	51.303	7.074	5.763	54.196
60	14.471	9.450	7.163	50.501	8.113	6.649	54.053
70	18.410	12.031	9.441	48.718	10.267	8.513	53.758
76	20.927	13.681	10.925	47.794	11.648	9.718	53.562

(c) Peak acceleration (cm/s<sup>2</sup>)

Building floor	Uncontrolled	TMD	PSO-TMD	Reduction (%)	ATMD	PSO-ATMD	Reduction (%)
55	13.352	9.923	8.208	38.526	7.539	6.256	53.145
60	16.804	11.835	9.369	44.245	7.522	6.687	60.205
70	19.851	12.855	12.764	35.701	9.153	8.691	56.219
76	27.825	22.332	19.797	28.852	11.905	9.370	66.325

Note: The reduction (%) is the PSO-TMD/PSO-ATMD w.r.t. uncontrolled.

As shown in Figs. 8–10 and Table 2, the reduction ratios w.r.t. the uncontrolled responses show that the PSO-based ATMD can control the wind-induced vibration of the high-rise structure better than the PSO-based TMD; in particular, it is most obvious by the comparison with the acceleration reduction, such as the 76 th floor where the reduction ratio reached 66%. Moreover, the proposed strategy effectively achieved the optimal parameters of TMD/ATMD, and the controlled responses were proved to be better than an empirical approach.

## 6 Conclusions

The application of DIT-FFT-WAWS was studied to achieve a simulated fluctuating wind load process of a high-rise building considering vertical correlation and as a result, the algorithm was proved to be simple and fast. Moreover, the accuracy can be effectively guaranteed. Compared to the Davenport spectrum, the simulated power spectral density function curves of fluctuating wind speed was highly consistent with the objective trend, thus providing a strong guarantee for accurate wind load simulation.

A novel PSO-based TMD (ATMD) controller was proposed for the reduction of the benchmark structure subjected to the simulated fluctuating wind. This study sets out to design and optimize the parameters of the TMD (ATMD) control scheme for achieving the best results in the reduction of a high-rise building. The design of the two controllers was formatted as an optimization problem based on the IAE performance index.

The numerical results show that both of the two controllers can effectively reduce wind-induced vibrations in tall buildings, and that the innovative method is applicable. Notably, the PSO-based ATMD performed better than the other, mainly because of the active controller in view of the almost identical optimal parameters of the mass damper system.

Along with artificial intelligence, the conventional control strategies of structure vibrations can be further improved using a specific performance index that can reflect typical characteristics of the controlled object, and this idea can not only solve the wind-induced vibration control, but also inspire other structural vibrations such as seismic vibration.

## Acknowledgments

This research was completely supported by National Natural Science Foundation of China, and the Grant Nos. are 51078123, 51179043. Valuable comments and suggestions by Professor ZHU Da-yong and XU Jian on the ideas carried out are gratefully acknowledged.

## References

- [1] Frahm, H.: U.S. Patent No. 989,958. Washington, DC: U.S. Patent and Trademark Office, 1911.
- [2] Rana, R., Soong, T. T.: *Parametric study and simplified design of tuned mass dampers*, Engineering structures, 20 (1998), 3, 193-204.
- [3] Carlo, M. G., Rita, C., Bernardino: *A comparison between different optimization criteria for tuned mass dampers design*, Journal of Sound and Vibration, 23 (2010), 329, 4880-4890.
- [4] Bekdaş, G., Nigdeli, S. M.: *Estimating optimum parameters of tuned mass dampers using harmony search*, Engineering Structures, 9 (2011), 33, 2716-2723.
- [5] Abdel-Rohman, M.: *Optimal design of active TMD for buildings control*, Building and Environment, 3 (1984), 19, 191-195.
- [6] Samali, B., Al-Dawod, M., Kwok, K. C. S., et al: *Active control of cross wind response of 76-story tall building using a fuzzy controller*, Journal of engineering mechanics, 130 (2004), 4, 492-498.
- [7] Iannuzzi, A., Spinelli, P.: *Artificial wind generation and structural response*, Journal of structural engineering, 113 (1987), 12, 2382-2398.
- [8] Lazzari, M., Saetta, A. V., Vitaliani, R. V.: *Non-linear dynamic analysis of cable-suspended structures subjected to wind actions*, Computers & Structures, 79 (2001), 9, 953-969.
- [9] Li, Y., Kareem, A.: *ARMA systems in wind engineering*, Probabilistic Engineering Mechanics, 5 (1990), 2, 49-59.
- [10] Torres, J. L., Garcia, A., De Blas, M., De Francisco, A.: *Forecast of hourly average wind speed with ARMA models in Navarre (Spain)*, Solar Energy, 79 (2005), 1, 65-77.

- [11] Shinozuka, M., Jan, C. M.: *Digital simulation of random processes and its applications*, Journal of sound and vibration, 25 (1972), 1, 111-128.
- [12] Yang, J. N.: *On the normality and accuracy of simulated random processes*, Journal of Sound and Vibration, 26 (1973), 3, 417-428.
- [13] Sun, Z.: *Computer simulation and analysis of wind loading of structures*, Dissertation, Nanjing university of aeronautics and astronautics, 2007.
- [14] Eberhart, R. C., Kennedy, J.: *A new optimizer using particle swarm theory*, In Proceedings of the sixth international symposium on micro machine and human science, Nagoya, 1995, 39-42.
- [15] Yang, J. N., Agrawal, A. K., Samali, B., Wu, J. C.: *Benchmark problem for response control of wind-excited tall buildings*, Journal of engineering mechanics, 130 (2004), 4, 437-446.
- [16] Design code: *Load code for the design of building structures*, Beijing, China, 2012.
- [17] Davenport, A. G.: *The relationship of wind structure to wind loading*, In Proceedings of the Symposium on Wind Effect on Building and Structures, London, 1965, 390-402.
- [18] Shi, Y., Eberhart, R.: *A modified particle swarm optimizer*, IEEE World Congress on Computational Intelligence, Anchorage, AK, 1998, 69-73.
- [19] Farshidianfar, A., Saghafi, A., Kalami, S. M., Saghafi, I.: *Active vibration isolation of machinery and sensitive equipment using control criterion and particle swarm optimization method*, Meccanica, 47 (2012), 2, 437-453.